JMBFS

Journal of Microbiology, Biotechnology and Food Sciences

International peer-reviewed scientific online journal

Published by Faculty of Biotechnology and Food Sciences

SOYBEAN-MEDIATED GREEN SYNTHESIS OF RGO/SIO₂/ZNO NANOCOMPOSITES FOR ANTIMICROBIAL PROTECTION AND SEED NANO-PRIMING ENHANCEMENT

Mohamed M. El-Zahed, Manal A. Abdelhamid, Mamdouh M. Nemat Alla, Enas G. Badran*

Address(es):
Department of Botany and Microbiology, Faculty of Science, Damietta University, New Damietta, Egypt.

*Corresponding author: mohamed.marzouq91@du.edu.eg

https://doi.org/10.55251/jmbfs.13967

ARTICLE INFO

Received 13. 2. 2026
Revised 15. 3. 2026
Accepted 25. 3. 2026
Published 1. 4. 2026

Regular article

OPEN ACCESS

ABSTRACT

Developing multifunctional nanomaterials remains critical for sustainable crop protection and the mitigation of biotic stress. This study describes the green synthesis of a ternary reduced graphene oxide/silicon dioxide/zinc oxide (rGO/SiO_2/ZnO) nanocomposite, utilizing an aqueous extract of soybean (*Glycine max*) as a sustainable reducing and stabilizing agent. FTIR spectroscopy confirmed the reduction of graphene oxide (GO) to rGO. Transmission electron microscopy (TEM) revealed the successful anchoring of crystalline ZnO and SiO_2 nanoparticles, with an average diameter of 55 nm, onto the rGO matrix. The stability of the synthesized architecture was validated by a zeta potential of -30.9 mV, indicating high colloidal stability. Biological assays demonstrated significant broad-spectrum antimicrobial efficacy. The nanocomposite achieved a 3.5-fold increase in the inhibition zone against *Escherichia coli* compared to monometallic ZnO NPs and exhibited significant inhibitory efficacy against *Fusarium oxysporum*, *Penicillium digitatum*, *Aspergillus niger*, and *Candida albicans*. Time-kill kinetics demonstrated rapid, concentration-dependent microbicidal efficacy, while TEM ultrastructural analysis of treated *F. oxysporum* revealed cellular degradation, characterized by expanded vacuoles and lipid droplet accumulation. In seed nano-priming experiments, soybean seeds treated with rGO/SiO_2/ZnO (50–500 mg/L) exhibited improved germination percentages and reduced disease incidence. The 150 mg/L concentration was identified as the optimal treatment, yielding a 57% increase in fungicidal action against *F. oxysporum* relative to ZnO NPs alone. Furthermore, this treatment mitigated pathogen-induced damage, resulting in a 400% increase in germination rate over infected controls and a 197% increase in shoot fresh mass compared to healthy, unprimed controls. These findings indicate that the rGO/SiO_2/ZnO nanocomposite exhibits a multifunctional profile, acting concurrently as a biostimulant and a protective agent. This suggests its potential as an integrated approach for managing fungal-induced biotic stress in soybean cultivation. This study provides a foundational step toward developing sustainable nanomaterials that may contribute to long-term crop resilience in agricultural systems.

Keywords: *Glycine max*, Green synthesis, rGO/SiO_2/ZnO, Antimicrobial activity, Time-kill kinetics, Ultrastructural analysis, Nano-priming, *Fusarium oxysporum*

INTRODUCTION

Recent years have seen a significant increase in the use of nanotechnology in agriculture, a rapidly evolving field, due to its potential and quick fixes that are essential for sustainable agriculture **(Atanda *et al*., 2025; Singh *et al*., 2025)**. Nanomaterials in general are promising materials for the site-specific delivery of nucleotides, proteins, and chemicals under *in vitro* settings to accomplish important goals, including enhancing crop development and yield and tolerance against stressful signals **(Banerjee *et al*., 2023)**. Nanoparticles (NPs) come in a wide variety of forms, and some are classified as helpful NPs because of their favorable effects on crop plants. Beneficial NPs that can be used as nutrients or as a nanocarrier for fertilizers are more effective than conventional fertilizers due to their unique mechanism of action, improved performance, novel physico-chemical properties, and low environmental pollution **(Shabiya *et al*., 2025)**.

Among NPs, zinc oxide nanoparticles (ZnO NPs) are one of the most manufactured NPs globally and used in agricultural applications **(Bouhadi *et al*., 2025; Kamal *et al*., 2024)**. Numerous industrial goods frequently contain ZnO NPs, where the size, concentration, exposure duration, and plant species are essential factors that influence ZnO NPs' efficacy **(Fayed *et al*., 2025; Sani *et al*., 2023; Pedruzzi *et al*., 2020)**. Numerous studies on the effects of ZnO NPs on plants' biomass, antioxidant activity, gas exchange, and chlorophyll content have been conducted in recent years **(Faizan *et al*., 2021; Wang *et al*., 2016)**. Plants require zinc (Zn) as a micronutrient, and agricultural soils all over the world frequently lack it **(Lindsay, 1972)**. Zn is essential for the function of several enzymes, is a crucial component of transcription factors belonging to the Zn finger family, and is crucial for the process of photosystem II repair. According to **Sharma *et al*. 2013**, a Zn deficit causes plants to grow less, be less able to handle stress, and produce less chlorophyll. In contrast, larger amounts of Zn can have hazardous consequences that are comparable to those of heavy metals. It encourages iron and magnesium insufficiency, the production of reactive oxygen species (ROS), and the removal of other metals from the active regions of proteins **(Sagardoy Calderón *et al*., 2009)**.

Both top-down and bottom-up approaches are used in the synthesis of nanomaterials **(Majumder *et al*., 2007)**. However, traditional nonbiological techniques (such as pyrolysis or sol-gel) frequently include hazardous reactants, high energy usage, and expensive expenses **(Guo *et al*., 2016)**. The biological techniques, sometimes referred to as "green synthesis," offer a more ecologically friendly option **(Salem and Fouda, 2021)**. This method is effective and friendly since it uses microorganisms or plant extracts to biosynthesize NPs, utilizing naturally available biomolecules to reduce and cap metal ions **(El-Zahed *et al*., 2023; Mohd Yusof *et al*., 2020)**. Several studies were conducted to green-synthesize ZnO NPs using different plant extracts **(Rafique *et al*., 2023; Ullah and Lim, 2022)**. However, to the best of our knowledge, there is no study that has used an aqueous extract of soybean in the green synthesis of ZnO NPs. As the most important source of vegetable oil and proteins, soybeans hold a prominent place among crops **(Budran *et al*., 2023)**. Except for sulfur-containing amino acids like methionine, soy proteins constitute the main source of plant-based proteins with well-balanced essential amino acids **(Li *et al*., 2025; Qin *et al*., 2022)**. Given the importance of the soybean plant in Egypt, it was targeted in this study as it has emerged as a viable agricultural solution, addressing challenges such as food security, import reliance, and economic diversification **(Naser *et al*., 2024)**. Different strategies are proposed to enhance Egypt's soybean agriculture, emphasizing breeding programs focused on high yields, disease resistance, and abiotic stress tolerance. The ability of the fabricated nanomaterials was also modulated to enhance the soybean growth.

The antimicrobial activity of NPs has improved recently through their combination with polymers, and they may be able to inhibit or eradicate germs without harming the surrounding tissue **(Baka and El-Zahed, 2022)**. Silica (SiO_2) and silicon (Si) reduce the harmful effects that different environmental pressures have on plants and are thought to be quasi-essential for plant growth and development **(Wang *et al*., 2016)**. According to **Kim *et al*. 2016**, SiO_2 is the second most prevalent element in soil after nitrogen. It is an essential part of crop production, particularly in reducing the adverse effects of oxidative, salinity, and drought stressors **(Seleiman *et al*., 2019)**. Applying nano-Si to plants improves their nutritional status by

reducing the movement of Na^+ ions from roots to leaves and raising the concentration of K^+ ions in leaves in salinized soil **(Youssif *et al*., 2018)**. Recently, it was shown that plants treated with nano-minerals as stimulants and nutrients exhibited enhanced biochemical and physiological characteristics, reduced oxidative damage, increased uptake of nutrients and water, and enhanced plant development, all of which led to higher seed yields **(Liu and Lal, 2015)**.

In agriculture, graphite (Gt) is essential because it acts as a soil conditioner, improving soil health and plant growth by increasing nutrient availability. Additionally, it can help seeds flow more easily during sowing and possibly increase fertilizer efficiency **(Qian *et al*., 2015)**. In order to create a sustainable cycle of resource consumption, it can be obtained from agricultural waste. It has the ability to raise soil organic carbon, which is essential for the cycling of nutrients and soil fertility in general **(Hindersah *et al*., 2018)**. According to Pandorf *et al*. **(Pandorf *et al*., 2020)**, nano-Gt may also improve plant productivity and soil nitrogen retention in addition to altering soil enzyme activity. Furthermore, Gt can be added to fertilizer coats, which could improve the way nutrients reach plants. Because of its special qualities and capacity to improve plant growth, nutrient absorption, and stress tolerance, graphene oxide (GO) has great promise for advancing agricultural methods **(Singh and Das, 2024)**. It can be used as a fertilizer, a clever way to transport pesticides and nutrients, and a tool to improve the antibacterial qualities and soil health **(Baka and El-Zahed, 2023)**. The makeup of soil microbial communities can be influenced by Gt and GO, which may have an effect on soil health and nutrient cycling.

The current study aimed to prepare and characterize the newly green-synthesized reduced graphene oxide/silicon dioxide/zinc oxide nanocomposite (rGO/SiO_2/ZnO), which was made of ZnO NPs and silica nanoparticles (SiO_2 NPs) decorated on the GO sheets. The antimicrobial activity of the fabricated nanocomposite against different microbial strains would also be investigated, and the relationships between the structural parameters of this nanocomposite and its antimicrobial activity were evaluated. Using agar well diffusion susceptibility tests and a broth dilution method, the antimicrobial activity investigation was conducted against the Gram-positive bacteria (*Bacillus paramycosides* and *Staphylococcus aureus*), the Gram-negative bacteria (*Escherichia coli* and *Salmonella typhi*), and the fungi (*Fusarium oxysporum*, *Penicillium digitatum*, *Aspergillus niger*, and *Candida albicans*). In addition, in a simple preliminary experiment, the new nanocomposite was applied to determine how to benefit from it in various agricultural applications as a fungicide. The ability of the fabricated nanocomposite to modulate soybean growth was studied using a priming experiment.

MATERIALS AND METHODS

Plant materials

The present investigation was conducted in the Physiology and Microbiology Laboratories of the Botany and Microbiology Department at the Faculty of Science, Damietta University, Egypt. The soybean [*Glycine max* (L.)] cultivar Giza 21 seeds were provided by the Agricultural Research Institute in Kafr El-Sheikh, Egypt. Healthy, uniformly sized seeds were carefully cleaned with water and then soaked overnight before being planted in pots measuring 18 x 15 x 12 inches filled with sand soil and placed in a greenhouse. The seeds were watered daily for seven days and then received Long Ashton nutrient solution for ten days **(Hudson, 1967)**.

Preparation of soybean leaf extract

The plant extract was prepared following the method described by **Shafey (2020)** with specific adjustments for the biosynthesis of NPs. Fresh leaves of soybean (*Glycine max*) were thoroughly washed, cut into small fragments, and ground to increase the surface area for extraction. The ground leaves were immersed in distilled water and maintained under constant agitation at 150 rpm for 24 hours at 25°C. To ensure the removal of cellular debris and obtain a high-purity extract, the resulting mixture was filtered through Whatman No. 1 filter paper, followed by centrifugation at 4000 ×g for 20 minutes. The clarified aqueous extract was then transferred to light-protected containers and stored at 4°C for use in subsequent green synthesis experiments.

Green synthesis of ZnO NPs

The biosynthesis of ZnO NPs was conducted following the procedure outlined by **Umar et al. (2019)** with slight modifications. Initially, 10 mL of *Glycine max* aqueous extract was slowly added to a 250 mL Erlenmeyer flask containing 90 mL of 0.1 M zinc nitrate hexahydrate [$Zn(NO_3)_2.6H_2O$]. The mixture was continuously stirred using a magnetic stirrer for three hours at 80°C. To aid in the precipitation of the NPs, the pH of the solution was monitored and kept between 9 and 10 by adding a sodium hydroxide (NaOH) solution. A noticeable color change from yellowish-green to yellowish-white occurred during the reaction, indicating the reduction and formation of the NPs. The resulting pale white precipitate was collected through centrifugation, washed several times with distilled water to eliminate any unreacted precursors or plant residues, and then dried in an oven at 70°C for eight hours. The synthesized ZnO NPs were stored for further characterization and integration into the composite.

Green synthesis of SiO_2 NPs

The synthesis of SiO_2 NPs was carried out using a sustainable green chemistry approach mediated by soybean extract. Initially, a 1 mM aqueous solution of sodium silicate was prepared, and the pH was adjusted to 6. This solution was then mixed with the soybean aqueous extract in a 1:1 (v/v) ratio. The mixture was agitated on a rotary shaker at 150 rpm at room temperature for 12 hours (overnight) until a characteristic color change to brown was observed, indicating the formation of the NPs. The resulting suspension was filtered using Whatman No. 1 filter paper to separate the produced NPs. To ensure crystallization and phase purity, the obtained material underwent calcination at 180°C for five hours in a muffle furnace, following the protocol described by **AL-Azawi et al. (2019)**. The final SiO_2 NPs were stored under desiccated conditions for further characterization and composite fabrication.

Synthesis of silicon/reduced graphene oxide nanocomposite (SiO_2/GO)

Commercial GO powder was sonicated for two hours in ethylene glycol (90 mL, Sigma Aldrich, 99%). Polyacrylic acid -functionalized GO (PAA-GO) was created by adding 2 g of low-molecular-weight polyacrylic acid (PAA) powder (Sigma Aldrich, mw ¼ 1800) to the suspension to promote the interaction of its carboxylic groups with the GO epoxy and hydroxyl moieties. This functionalization increased the interlayer gap between GO planes and decreased the restacking propensity of GO sheets. The PAA-GO mixture was sonicated for an additional hour before adding SiO_2 NPs (0.1 g) and diluting them in distilled water. Further sonification for two hours allowed the SiO_2 to disperse throughout the PAA-GO framework. The homogeneity of the suspension after 20 minutes of stirring at 90°C indicated that SiO_2 NPs were anchored between the expanded GO sheets of the partially reduced PAA-GO. Any excess of undispersed SiO_2 or PAA that was not trapped in the GO matrix was removed from the solution by filtering and cleaning it. The resulting powder was dried by baking it at 50°C overnight **(Maroni *et al*., 2014)**.

Decoration of ZnO NPs onto SiO_2/GO

The integration of ZnO NPs onto the SiO_2/GO matrix was performed using a modified decoration method (Jafari *et al*., 2018). Initially, ZnO NPs and SiO_2/GO were independently re-dispersed in distilled water and subjected to ultrasonication for one hour to ensure uniform dispersion. The two suspensions were then combined and stirred at 50°C for 30 minutes. To facilitate the final assembly and the reduction of GO, a 0.2 M NaOH solution was added dropwise to the mixture under constant stirring until an alkaline environment (pH 8) was achieved. The temperature was then increased to 95°C and maintained for 20 minutes, resulting in a white, gelatinous suspension. This process ensured the successful anchoring of the NPs onto the rGO framework. The resulting rGO/SiO_2/ZnO nanocomposite was collected by centrifugation, washed, and dried at 80°C for three hours to obtain a fine greyish powder. The comprehensive green synthesis pathway and the structural assembly of the rGO/SiO_2/ZnO are schematically illustrated in Fig. 1.

Characterization of the rGO/SiO_2/ZnO nanocomposite

Fourier transform-infrared (FT-IR) (FT/IR-4100typeA), and ultraviolet-visible (UV/VIS/NIR Spectrophotometer V-630, Japan) spectra were utilized to characterize the manufactured nanomaterials. Transmission electron microscopy (TEM) (JEOL JEM-2100, Japan), a zeta sizer and zeta potential (Malvern Instruments Ltd; zs90, Worcestershire, UK), as well as X-ray diffraction pattern (XRD) (model LabX XRD-6000, Shimadzu, Japan) were used to analyze the physical characteristics of the prepared nanomaterials.

Antimicrobial activity using the agar well diffusion method

The antimicrobial potential of the synthesized rGO/SiO_2/ZnO nanocomposite was evaluated using the agar well diffusion method across diverse microbial strains compared to GO, ZnO NPs, and SiO_2 NPs, following CLSI guidelines **(CLSI, 2017)**. Briefly, microbial suspensions (0.5 McFarland) were inoculated via the pour plate method onto Müller-Hinton agar (bacteria), potato dextrose agar (fungi), or Sabouraud dextrose agar (yeast). Wells of 6 mm diameter were loaded with 100 µL of the nanocomposite (150 µg/mL). Ampicillin and Fluconazole served as positive controls at equivalent concentrations. Following appropriate incubation periods (48 hours at 37°C for bacteria/yeast; 5 days at 28°C for fungi), the zones of inhibition were measured to quantify antimicrobial efficacy.

Minimum inhibitory concentration (MIC)

The MICs for the monometallic NPs, the rGO/SiO_2/ZnO nanocomposite, and the positive controls were determined using the broth microdilution method in 96-well microtiter plates, following the protocol described by **Patel *et al.* (2011)**. Each microbial strain was standardized to a 0.5 McFarland turbidity standard

(approximately 1.5×10^8 CFU/mL) in appropriate broth media. Serial dilutions of the antimicrobial agent and positive controls were prepared to achieve a concentration range of 0 to 100 µg/mL. Each well was inoculated with the microbial suspension and incubated at the optimal temperature for each strain (37°C for bacteria and 28°C for fungi) for 24–48 hours. Following incubation, microbial growth was assessed by observing turbidity and comparing it with both positive (inoculated medium without treatments) and negative (sterile medium) growth controls to identify the lowest concentration that completely inhibited visible growth.

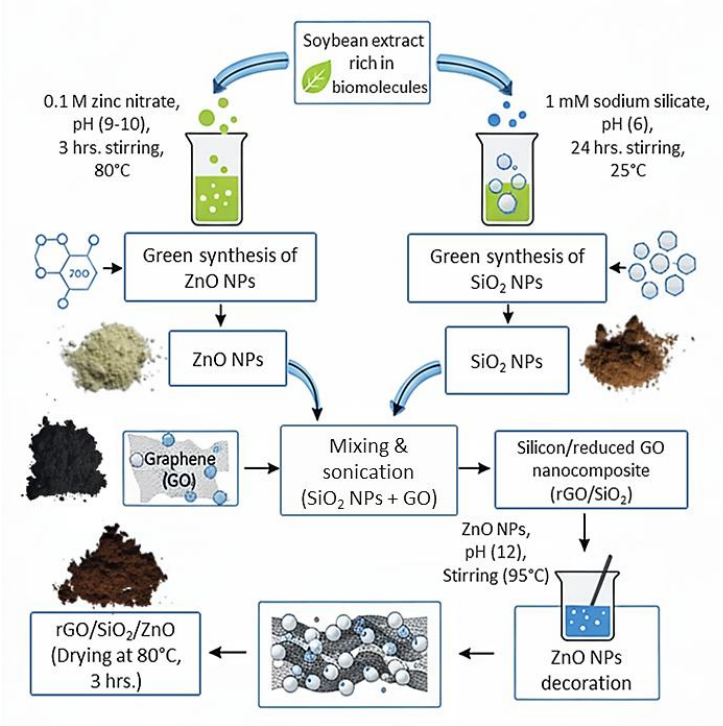

Fig. 1 Sequential steps for the green synthesis of ZnO-loaded rGO/SiO_2 (rGO/SiO_2/ZnO).

Time-kill kinetic assay

The time-kill kinetics were performed against *B. paramycosides*, *E. coli*, and *C. albicans* to evaluate the dynamic antimicrobial efficacy of the rGO/SiO_2/ZnO nanocomposite compared to other treatments (GO, ZnO NPs, and SiO_2 NPs). The procedure followed the guidelines described by CLSI with minor modifications **(CLSI, 1999)**. Fresh cultures were adjusted to a 0.5 McFarland standard in Mueller-Hinton broth (for bacteria) and Sabouraud dextrose broth (for *C. albicans*). The microbial suspensions were treated with the antimicrobial agent at concentrations corresponding to 1 × MIC and 2 × MIC. A growth control (untreated) was maintained for both strains. Aliquots (100 µL) were collected at specific time intervals: 0, 2, 4, 8, 12, and 24 hours of incubation at 37°C. Samples were serially diluted in sterile saline (0.9% NaCl), plated onto agar media, and incubated for 24 hours. The number of viable colonies was recorded as $\log_{10}$ CFU/mL. Bactericidal and fungicidal activity was defined as a ≥ 3-$\log_{10}$ reduction in CFU/mL compared to the initial inoculum. All assays were performed in biological triplicate.

Ultrastructural analysis

To visualize the internal morphological changes in *F. oxysporum* following treatment with the rGO/SiO_2/ZnO nanocomposite, TEM was employed according to the protocol described by Hayat (1981) with specific modifications for fungal hyphae. Mycelial plugs from the edge of an actively growing culture were treated with the nanocomposite at its MIC for 24 hours. Untreated mycelia served as the negative control. Samples were fixed in 2.5% (v/v) glutaraldehyde in 0.1 M phosphate buffer (pH 7.2) for 24 hours at 4°C, followed by post-fixation in 1% osmium tetroxide for 2 hours. Hyphae were dehydrated through a graded ethanol series (30%–100%) and embedded in epoxy resin. Ultra-thin sections were cut using an ultramicrotome, collected on copper grids, and double-stained with uranyl acetate and lead citrate. The ultrastructure was examined using a TEM (JEOL JEM-2100, Japan).

Seed nano-priming and pathogen challenge

To evaluate the protective effects of the rGO/SiO_2/ZnO nanocomposite, soybean seeds were first surface-sterilized with sodium hypochlorite (NaOCl) and rinsed thoroughly. For the pathogen challenge, seeds were immersed in a *F. oxysporum* spore suspension (10^6 CFU/mL) for 8 hours at 25°C in darkness. After drying to their original moisture content, the infected seeds underwent nano-priming by immersion in rGO/SiO_2/ZnO suspensions (50, 150, and 500 mg/L) for 6 hours. The germination assays were conducted using a completely randomized design. Each treatment consisted of three biological replicates, with 40 seeds per replicate. Seeds were maintained at 25°C for 10 days, during which the germination percentage and seedling vigor index (length, fresh mass, and dry mass) were recorded.

Statistical analysis

All experimental procedures were conducted in three independent biological replicates (n=3) to ensure reproducibility. Statistical analysis was performed using SPSS software (Version 18.0). Before mean comparisons, the normality of data distribution and homogeneity of variances were verified using the Shapiro-Wilk and Levene's tests, respectively. Significant differences between treatment groups (e.g., control, monometallic NPs, and nanocomposite) were evaluated using a one-way analysis of variance (ANOVA). For post-hoc pairwise comparisons, Tukey's Honestly Significant Difference (HSD) test was utilized to determine specific differences between means, as it provides a more conservative control of the experiment-wise error rate. Data are presented as the mean ± standard deviation (SD), and a p-value < 0.05 was considered the threshold for statistical significance.

RESULTS AND DISCUSSION

Characterization of the prepared nanomaterials

The UV-vis spectra of SiO_2 NPs, ZnO NPs, and rGO/SiO_2/ZnO nanocomposite are shown in Fig. 2. The characteristic π–π* transitions of the aromatic C-C bonds in the graphene framework are typically identified by a peak near 230 nm. While SiO_2 NPs, being wide-bandgap insulators ($E_g \approx 9$ eV), showed an absorption edge at 264 nm, the ZnO NPs exhibited a sharp, well-defined excitonic absorption peak at 320 nm **(Musa and Qamhieh, 2019)**. This position is blue-shifted relative to bulk ZnO (359 nm), providing clear evidence of quantum confinement in the synthesized NPs **(de Medeiros *et al*., 2021; Kumar *et al*., 2019)**. In the rGO/SiO_2/ZnO nanocomposite spectrum, the emergence of a surface plasmon resonance-like feature at 354 nm signifies the successful integration of ZnO and SiO_2 onto the rGO sheets. Notably, the sharp excitonic peak of isolated ZnO is lost in the nanocomposite, replaced by a broad shoulder in the 330–360 nm region (Ahmed *et al*., 2018). This broadening and loss of sharpness are attributed to the formation of new electronic states at the interfaces between the ZnO NPs, the SiO_2 phase, and the rGO matrix, which smears out the discrete quantum confinement effects seen in the isolated particles. Also, **Naghani *et al*. (2023)** recorded two absorption peaks at 230 nm and 366 nm due to the GO and ZnO NPs, respectively. While **Ain *et al*. (2018)** found a broad peak occurring at 230-270 nm for GO-Si.

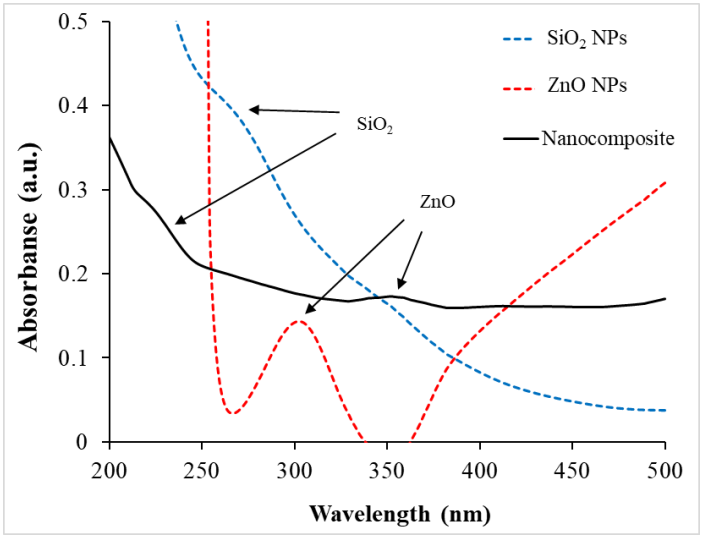

Figure 2 UV-vis absorption spectra of SiO_2 NPs, ZnO NPs, and the rGO/SiO_2/ZnO nanocomposite. The spectra illustrate the characteristic excitonic absorption peak of ZnO at 320 nm. The ternary nanocomposite exhibits a significant red shift and an enhanced broadband absorption profile across the UV-visible range, suggesting electronic coupling and optical synergy between the rGO matrix and the anchored oxide NPs.

FT-IR spectroscopy displayed the chemical bonding and synergistic interaction between the rGO support and the inorganic nanofillers (Fig. 3). The near-total absence of the strong C=O carbonyl stretching peak (typically at 1720 cm^{-1}) suggests that the soybean extract effectively reduced GO to rGO during synthesis (Gijare *et al*., 2023). The SiO_2 spectrum is dominated by the asymmetric Si-O-Si stretching at 1080 cm^{-1} and surface Si-OH groups at 950 cm^{-1} **(Al-Rawashdeh *et al*., 2020)**. ZnO is identified by the characteristic Zn-O stretching vibration below

550 cm^{-1} **(Karthiga *et al*., 2025)**. The successful architecture of the rGO/SiO_2/ZnO is evidenced by specific spectral shifts. The reduction in intensity and broadening of the C=C aromatic vibrations (1625 cm^{-1}) and the C-O-C epoxy stretching (1260 cm^{-1}) indicate the involvement of these sites in NPs anchoring **(Toselli *et al*., 2015)**. The overlapping and shifting of peaks in the 900–1200 cm^{-1} region suggest the formation of interfacial Si-O-C bonds, resulting from the reaction between silanol groups on SiO_2 and the residual oxygen functional groups on the rGO backbone. The slight shift of the Zn-O peak toward higher wavenumbers suggests that ZnO is not merely physically mixed but is coordinated to the rGO/SiO_2 framework.

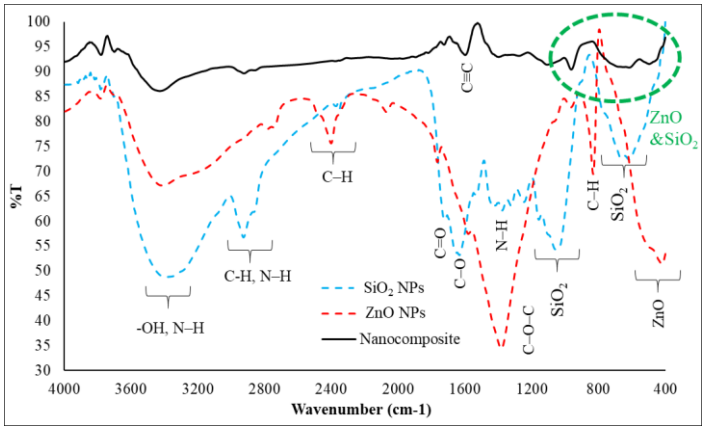

Figure 3 FT-IR Spectra of SiO_2 NPs, ZnO NPs, and the rGO/SiO_2/ZnO. The nanocomposite spectrum successfully merges the characteristic Si-O-Si stretching of SiO_2 (1080 and 604 cm^{-1}) and the Zn-O stretching (below 550 cm^{-1} onto the rGO matrix (C=C stretching at 1625 cm^{-1}). The absence of the C=O stretching vibration at 1720 cm^{-1} indicates the successful reduction of GO to rGO by the *Glycine max* extract, reflecting the removal of oxygen-containing functional groups during the green synthesis process. The shifts and broadening in the Si-O and C-O-C regions (≈950 - 1260 cm^{-1}) serve as strong evidence for the formation of interfacial bonding between the rGO backbone and the inorganic NPs.

The XRD pattern of the rGO/SiO_2/ZnO shows highly crystalline peaks at 2θ = 26.616°, 42.591°, 44.689°, 54.688°, and 77.596° (Fig. 4). The high crystallinity of ZnO and SiO_2 is responsible for the decoration of NPs on GO sheets in the presence of an alkaline medium. The drying process eliminated the distinctive peak of rGO. The ZnO crystalline peaks observed at 44.689°, 54.688°, and 77.596° corresponded to the lattice planes (102), (110), and (202) (JCPDS No. 36–1451). The XRD pattern of SiO_2 NPs (JCPDS No. 47-0715) displayed prominent diffraction peaks at 2θ = 8.866°, 25.489°, 26.616°, and 42.591°, corresponding to the lattice planes (200), (210), (011), and (211). These measured diffraction peaks aligned with findings from Goswami & Mathur (Goswami and Mathur, 2022) and El-Nour *et al*. (Abd El-Nour *et al*., 2023), supporting the crystalline structure of ZnO NPs and SiO2 NPs, respectively. Impurity-related diffraction peaks, not visible in the XRD graph, were used to validate the high purity. XRD analysis was utilized to investigate the typical crystal size and composition of the NPs integrated over GO sheets, providing a comprehensive overview of the crystal states mentioned. The NPs' size was determined using the Scherrer equation ($D = k\lambda/\beta cos\theta$), resulting in an average size of 55 nm.

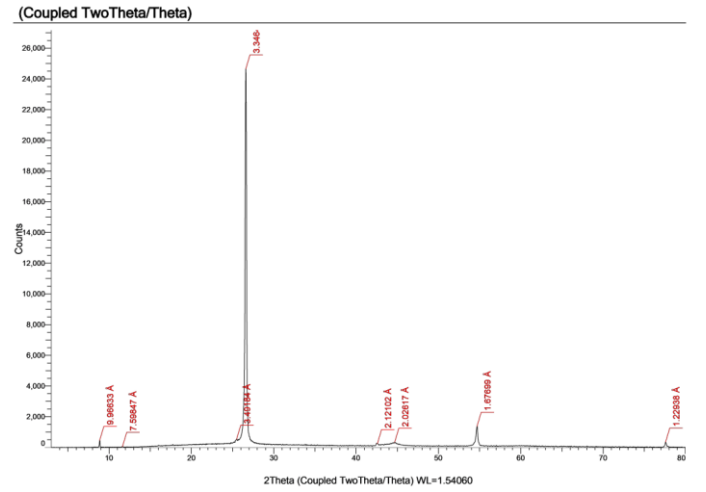

Figure 4 X-ray diffraction pattern of rGO/SiO_2/ZnO.

SiO_2 NPs and ZnO NPs were successfully loaded onto the monolayered GO sheets, as shown by TEM (Fig. 5). The image clearly displays a large, crumpled, sheet-like structure with varying degrees of transparency. This morphology is characteristic of rGO sheets. The presence of folds and ripples is characteristic of the material's two-dimensional (2D) nature and suggests the retention of a high effective surface area following functionalization. With a scale bar of 2 µm, the visible rGO flake in the image is several micrometers wide, demonstrating the successful exfoliation of GO into large, monolayer or few-layer sheets. Distributed NPs across the transparent rGO sheet are numerous, distinct, dark, quasi-spherical spots. The NPs appear as spherical-like particles with an average size between 33 and 78 nm. The average diameter of the spherical NPs was calculated using Nano Measurer 1.25 software and recorded as 55 ± 2.3 nm, which is in excellent agreement with the mean crystallite size of 55 nm as determined by the Scherrer equation. The TEM micrographs strongly suggest the formation of a genuine ternary nanocomposite rather than a simple physical mixture, as evidenced by the intimate interfacial contact and homogeneous distribution of the ZnO and SiO_2 NPs across the rGO sheets. The NPs are observed to be strongly anchored to the rGO surface and are not merely clumped together away from the sheet. According to several researchers, different plant extracts were used to generate ZnO NPs and SiO_2 NPs with a spherical shape and a size range of 50–108.5% **(Baka *et al*., 2024; Elumalai and Velmurugan, 2015; Madan *et al*., 2016; Sri Sindhura *et al*., 2014)**.

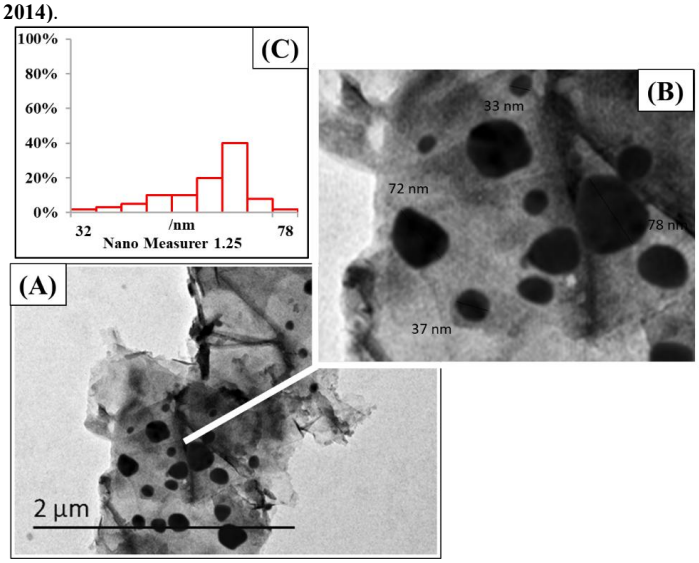

Figure 5 (A) TEM micrograph of rGO/SiO_2/ZnO. The micrographs illustrate the sheet-like, rippled morphology indicative of rGO nanosheets, where the observed wrinkling points to a high degree of structural flexibility and surface availability. Dark, quasi-spherical NPs ZnO or SiO_2) are observed to be anchored and distributed across the surface of the rGO backbone. The close physical association between the particles and the rGO sheets validates the formation of the desired heterogeneous structure necessary for synergistic applications. (B) The magnified part showed the spherical-like NPs with a particle range of 33-78 nm. (C) Nanogravimetric image showing the particle size distribution. Scale bar = 2 µm.

Fig. 6 illustrates that the zeta potential of the rGO/SiO_2/ZnO nanocomposite is -30.9 ± 10.4 mV. This high absolute value (exceeding the ± 30 mV threshold) indicates strong electrostatic repulsion between the particles, which is a key indicator of high colloidal stability. The negative surface charge is primarily attributed to the residual oxygen functional groups (such as carboxyl and hydroxyl groups) on the rGO sheets and the silanol (Si-OH) groups on the SiO_2 surface. This systematic electrostatic stabilization prevents the significant agglomeration often seen in unmodified metallic or metal-oxide NPs, ensuring a uniform dispersion of the nanocomposite in the aqueous medium. **Rosnan *et al*. (2018)** created a ZnO-decorated GO nanocomposite material with ZnO NPs using the sol-gel process, which has a zeta potential value of -28.23 mV **(Mahdavi *et al*., 2022)**. Chemically prepared GO/SiO_2 and GO/ZnO.

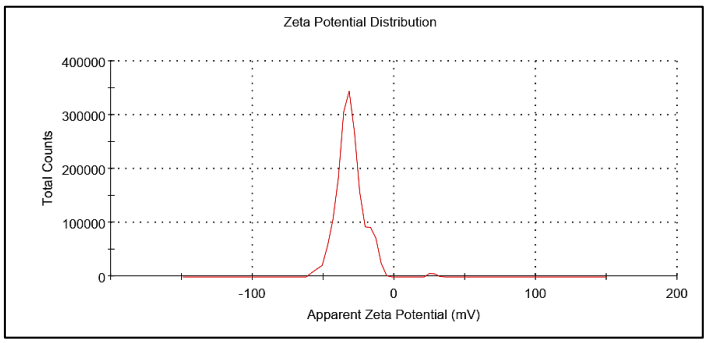

Figure 6 Zeta potential of rGO/SiO_2/ZnO, indicating the presence of a negative surface charge − 30.9±10.4 mV.

Antimicrobial activity

The antimicrobial efficacy of the synthesized ternary nanocomposite was assessed against clinically relevant pathogens, including Gram-positive bacteria (*S. aureus*, *B. paramycosides*), Gram-negative bacteria (*E. coli*, *S. Typhi*), and the yeast *C. albicans*. These strains were chosen due to their association with medically linked infections and antibiotic resistance **(Simões *et al*., 2010)**. As shown in Fig. 7 and Table 1, the biosynthesized reduced rGO/SiO_2/ZnO nanocomposite exhibited significant antimicrobial activity. Overall, the nanocomposite demonstrated greater effectiveness than the individual components (GO, ZnO NPs, and SiO_2 NPs), with efficacy levels comparable to positive controls such as ampicillin and fluconazole (Table 1). The nanocomposite showed the largest zones of inhibition against *B. paramycosides* (18 ± 0.03 mm) and *E. coli* (21 ± 0.14 mm). Particularly noteworthy is its activity against *E. coli,* which was 3.5 times higher than that of pure ZnO NPs (6 ± 0.14 mm). This synergistic enhancement is credited to the rGO backbone, which acts as a high-surface-area framework that prevents NPs aggregation and enables multiple antimicrobial mechanisms. These results are consistent with **El-Zahed *et al*. (2024)**, who reported promising activity of rGO/ZnO composites against *E. coli* and *C. albicans* compared to traditional agents. Similarly, **Elbasuney *et al*. (2021)** and **Bhaisare *et al*. (2016)** recorded the increased susceptibility of Gram-negative bacteria to these nanocomposites. The observed variation in susceptibility between Gram-negative and Gram-positive bacteria is likely connected to cell wall topology; the thick peptidoglycan layer of Gram-positive bacteria may offer more resistance to penetration compared to the thinner, lipopolysaccharide-shielded membrane of Gram-negative bacteria (Liu *et al*., 2011). Furthermore, the nanocomposite exhibited significant activity against fungal strains, particularly *Fusarium oxysporum* (22 ± 0.14 mm) and *Aspergillus niger* (20 ± 0.14 mm), achieving efficacy comparable to Fluconazole.

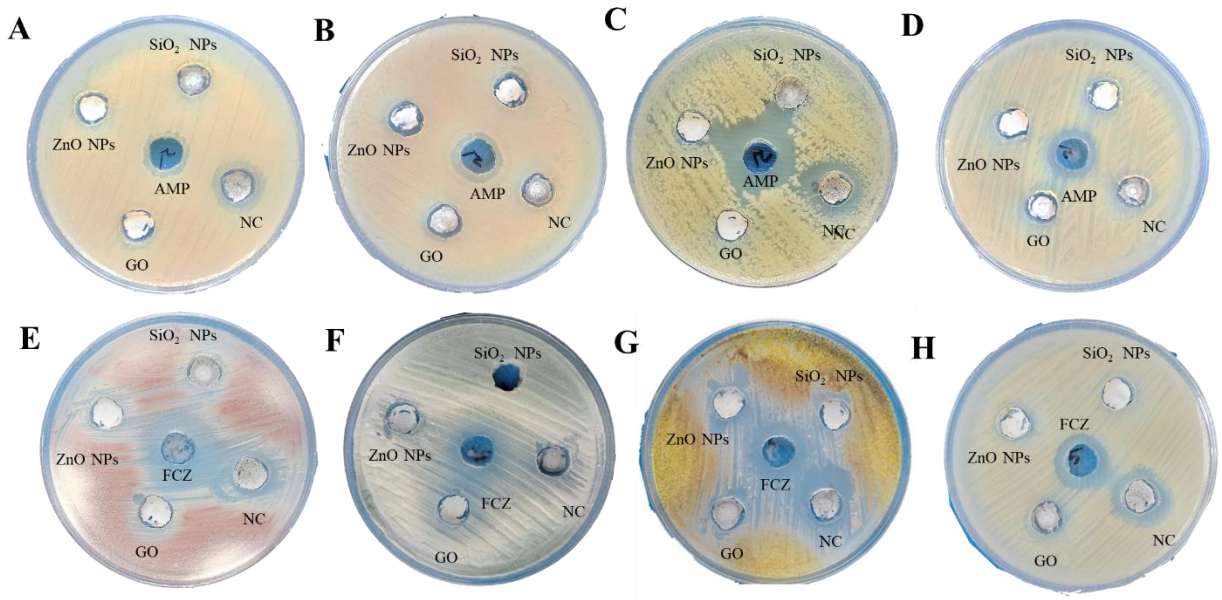

Figure 7 Antimicrobial activity of rGO/SiO_2/ZnO nanocomposite (NC), compared to ZnO NPs, SiO_2 NPs, GO, ampicillin (AMP), and fluconazole (FCZ) against *Bacillus paramycosides*; (A), *S. aureus*; (B), *E. coli*; (C), *S. typhi*; (D), *F. oxysporum*; (E), *P. digitatum*; (F), *A. niger*; (G), and *C. albicans*; (H).

Table 1 Antimicrobial activity of green synthesized rGO/SiO_2/ZnO and its individual components using the agar well diffusion method.

Antimicrobial agent	**Zone of inhibition (mm ± SD)**							
	Gram-positive bacteria		Gram-negative bacteria		Fungi			Yeast
	B. paramycosides	*S. aureus*	*E. coli*	*S. typhi*	*F. oxysporum*	*P. digitatum*	*A. niger*	*C. albicans*
GO	$7 \pm 0.14^{c*}$	8 ± 0.03^{e}	N.A.	11 ± 0.06^{c}	13 ± 0.06^{c}	11 ± 0.14^{c}	11 ± 0.14^{c}	12 ± 0.03^{c}
ZnO NPs	9 ± 0.06^{d}	8 ± 0.06^{e}	6 ± 0.14^{c}	10 ± 0.14^{d}	14 ± 0.03^{b}	8 ± 0.14^{d}	13 ± 0.14^{b}	10 ± 0.03^{d}
SiO_2 NPs	8 ± 0.06^{e}	7 ± 0.14^{f}	N.A.	9 ± 0.06^{e}	13 ± 0.14^{c}	N.A.	10 ± 0.14^{d}	N.A.
rGO/SiO_2/ZnO	18 ± 0.03^{b}	14 ± 0.14^{b}	21 ± 0.14^{b}	12 ± 0.14^{b}	22 ± 0.14^{b}	13 ± 0.14^{b}	20 ± 0.14^{a}	19 ± 0.06^{a}
Antibiotics#	15 ± 0.14^{c}	16 ± 0.03^{a}	24 ± 0.06^{a}	14 ± 0.06^{a}	26 ± 0.06^{a}	16 ± 0.14^{a}	20 ± 0.14^{a}	18 ± 0.14^{b}

**Values are expressed as mean ± SD (n = 3 biological replicates). Means within each column followed by different superscript letters are significantly different (p ≤ 0.05) according to Tukey's HSD test. N.A.: No Activity (Inhibition zone < 6 mm). #Positive controls: Ampicillin for bacteria and fluconazole for fungi/yeast.*

Minimum inhibitory concentration

The MIC is defined as the lowest concentration of an antimicrobial agent that prevents detectable microbial growth. Fig. 8 illustrates the MIC values of the reduced rGO/SiO_2/ZnO nanocomposite compared to its individual components: ZnO NPs, SiO_2 NPs, and GO. The results indicated that the MIC values for the individual components were generally higher than those for the nanocomposite across most tested strains. For GO, MIC values ranged from 110 to 140 µg/mL against fungal strains and 130 to 150 µg/mL against bacterial strains. Similarly, ZnO NPs exhibited MIC values between 110–140 µg/mL for fungi and 140–150 µg/mL for bacteria, while SiO_2 NPs showed values around 140–150 µg/mL. In contrast, the ternary nanocomposite exhibited significantly lower MIC values, recorded at ≥50 µg/mL against Gram-negative bacteria (*E. coli* and *S. typhi*) and ≥80 µg/mL against Gram-positive bacteria (*B. paramycosides* and *S. aureus*). For fungal action, including *C. albicans*, the MIC values for the nanocomposite ranged from 30 to 70 µg/mL. These findings suggest that the integration of ZnO NPs into the composite structure promotes the antimicrobial activity, which is consistent with previous observations by **Chowdhuri *et al*. (2015)**. The differential susceptibility observed between bacterial groups may be attributed to variations in their cell wall architectures. Gram-negative bacteria were found to be more susceptible to the rGO/SiO_2/ZnO nanocomposite, while the denser peptidoglycan layer in the cell walls of Gram-positive bacteria may provide a higher level of resistance **(El-Fallal *et al*., 2023)**. Additionally, the increased activity of the nanocomposite is likely influenced by the size and surface area of the NPs. The TEM results from this study showed a narrow size range for the synthesized NPs. According to **Stanković *et al*. (2013)**, smaller NPs typically demonstrate higher bioactivity due to their increased surface area-to-volume ratio, which augments interaction with microbial membranes.

Dynamic Killing Efficacy

The time-kill analysis revealed a potent, concentration-dependent microbicidal effect for the rGO/SiO_2/ZnO nanocomposite against both tested pathogens (Fig. 9). The growth control of bacterial strains reached its stationary phase within 12 hours. In contrast, the 1 × MIC treatment exhibited a steady decline in viability, achieving a 3-log reduction within 8 hours. The 2 × MIC treatment showed a rapid bactericidal effect, with no detectable viable cells observed after 18 hours of exposure. The killing kinetics of rGO/SiO_2/ZnO nanocomposite against *C. albicans* were slightly slower but equally effective. The 1 × MIC dose suppressed yeast growth significantly compared to the control. At 2 × MIC, the nanocomposite achieved a fungicidal state by the 18-hour mark, demonstrating its ability to compromise the more complex eukaryotic cell wall of the yeast. The kinetic data

elucidate the multifunctional properties of the rGO/SiO_2/ZnO architecture, providing a quantitative basis for its concurrent antimicrobial and biostimulatory performance. While the inhibition zone tests provided a snapshot of efficacy, the time-kill assay demonstrates that the material doesn't just inhibit growth—it actively eradicates cells. The rapid decline in *E. coli* viability (within 4 hours at 2 × MIC) supports the proposed hypothesis of immediate physical membrane disruption. The sharp peripheral edges of the rGO sheets—associated with the peripheral edge interaction mechanism—are hypothesized to initiate mechanical structural damage to the microbial membranes. This initial disruption may be further exacerbated by the localized release of Zn^{2+} ions and the putative generation of surface-bound ROS, consistent with synergistic models of nanocomposite toxicity **(Chowdhuri *et al.*, 2015)**. For *C. albicans*, the delayed but steady killing rate suggests that the nanocomposite must first overcome the chitinous cell wall. The integration of SiO_2 likely serves as a crucial stabilizer, ensuring a sustained release of active species over 24 hours. These results align with recent findings by **Amama & Adeoye (2026)**, **Elemike & Ivwurie (2020)**, **Gautam *et al.* (2024)**, and **Sani *et al.* (2023)**, who noted that ternary metal-carbon heterojunctions provide superior kinetic profiles compared to pristine ZnO NPs due to enhanced electron transfer and higher surface area contact.

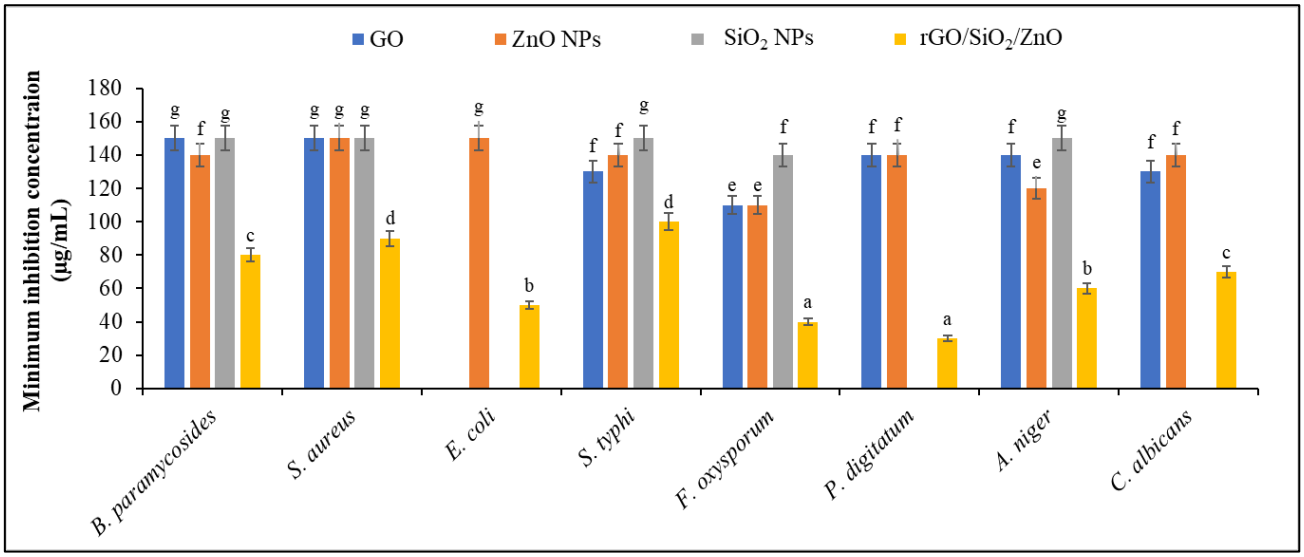

Figure 8 Minimum inhibitory concentrations of the rGO/SiO_2/ZnO nanocomposite compared to monometallic ZnO NPs, SiO_2 NPs, and GO. Data are presented as mean ± SD (n=3 biological replicates). Error bars labeled with different lowercase letters indicate significant differences at $p < 0.05$ according to Tukey's HSD test. The absence of bars for certain components (e.g., *E. coli* and *P. digitatum*) indicates no inhibitory activity within the tested concentration range (>150 µg/mL).

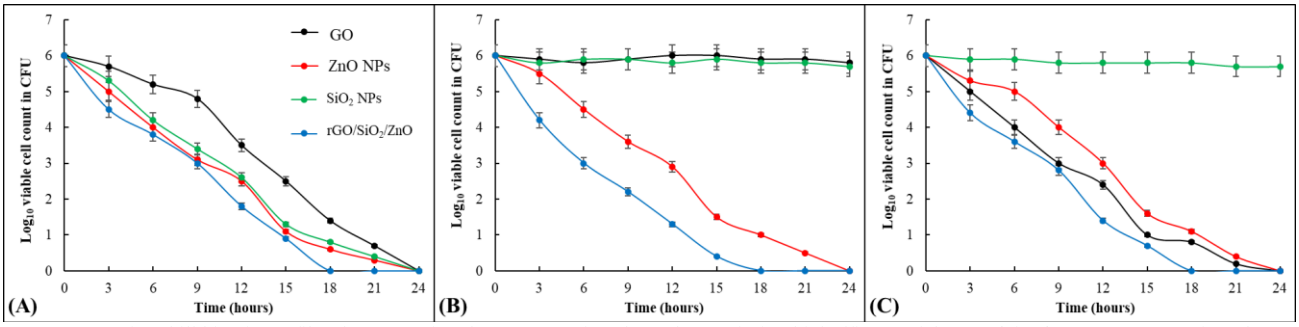

Figure 9 Time-kill kinetic profiles demonstrating the concentration-dependent antimicrobial efficacy of the rGO/SiO_2/ZnO nanocomposite. The survival curves illustrate the dynamic response of (A) *B. paramycosides*, (B) *E. coli*, and (C) *C. albicans* when exposed to concentrations of 2 × MICs compared to an untreated growth control. Data points represent the mean ± SD (n = 3).

Ultrastructural alterations study

The TEM micrographs revealed profound differences in the cellular integrity of *F. oxysporum* between the control and treated groups (Fig. 10). The untreated fungal cells exhibited a healthy and well-defined architecture (Fig. 10A). A distinct, rigid cell wall and an intact, continuous plasma membrane were observed. The cytoplasm appeared dense and compact, containing normal, small vacuoles and regularly distributed organelles, reflecting active metabolic health. On the other hand, significant structural degradation was evident following exposure to the rGO/SiO_2/ZnO nanocomposite (Fig. 10B). The appearance of a prominent extracellular mucilage substance was noted, effectively gluing or connecting adjacent hyphae, likely as a defensive stress response. The formation of abnormally large, expanded vacuoles indicates a disruption in osmotic balance and internal cellular pressure. A high accumulation of lipid droplets was observed in the cytoplasm, suggesting severe metabolic stress and potential lipid peroxidation of the membrane systems. The transition from the compact, organized cytoplasm of the control to the disorganized, lipid-heavy state of the treated samples provides clear evidence of cytotoxicity. The presence of lipid droplets and enlarged vacuoles is particularly telling. In fungal pathology, the accumulation of lipid bodies is a recognized hallmark of stress, often resulting from the breakdown of membrane phospholipids due to ROS or enzymatic disruption **(Nour El-Dein et al., 2021; Umar *et al.*, 2019)**. This supports our hypothesis that the nanocomposite triggers oxidative stress within the fungal cell. Furthermore, the observed secretion of mucilage-like substances may represent a protective stress response by *F. oxysporum*, potentially serving to encapsulate the nanocomposite particles or buffer the mycelia against the mechanical peripheral edge interaction of the rGO sheets. However, the internal damage—specifically the loss of cytoplasmic density—indicates that these defensive measures are insufficient. These findings are consistent with studies by **El-Zahed *et al.* (2022)** and **Wang *et al.* (2016)**, which observed similar organelle degradation in fungi exposed to metal and metal-oxide heterojunctions, reinforcing the conclusion that our ternary nanocomposite acts through a combination of physical membrane compromise and internal metabolic collapse.

Protection and enhancement of soybean seedling vigor using rGO/SiO_2/ZnO

The efficacy of the rGO/SiO_2/ZnO nanocomposite in mitigating *F. oxysporum*-induced stress is detailed in Fig. 11. The fungal pathogen significantly suppressed germination, reducing it from 60% (healthy control) to 18% (infected control). Nano-priming treatments demonstrated a systematic restorative effect; notably, the 150 mg/L treatment increased the germination rate to 84%—a 400% improvement over the infected control. In the post-germination phase, the 150 mg/L dose was identified as the optimal concentration, resulting in a 197% and 200% increase in fresh and dry mass, respectively, compared to the healthy control. Furthermore, this treatment normalized the root/shoot ratio to 0.20, counteracting the developmental shift toward excessive root growth (0.45) observed in stressed plants.

The data reveal a hormetic response typical of engineered nanomaterials. While the 150 mg/L concentration provided maximum growth promotion, a slight decline in germination (to 80%) was observed at the 500 mg/L concentration. This suggests

that while the nanocomposite is highly effective at moderate doses, higher concentrations may trigger concentration-dependent phytotoxicity or osmotic stress. Identifying this therapeutic window (150 mg/L) is critical for agricultural applications to ensure antimicrobial protection without compromising plant health, a trend consistent with previous studies on ZnO NPs-mediated antioxidant activity in chickpeas **(Farhana et al., 2022)**.

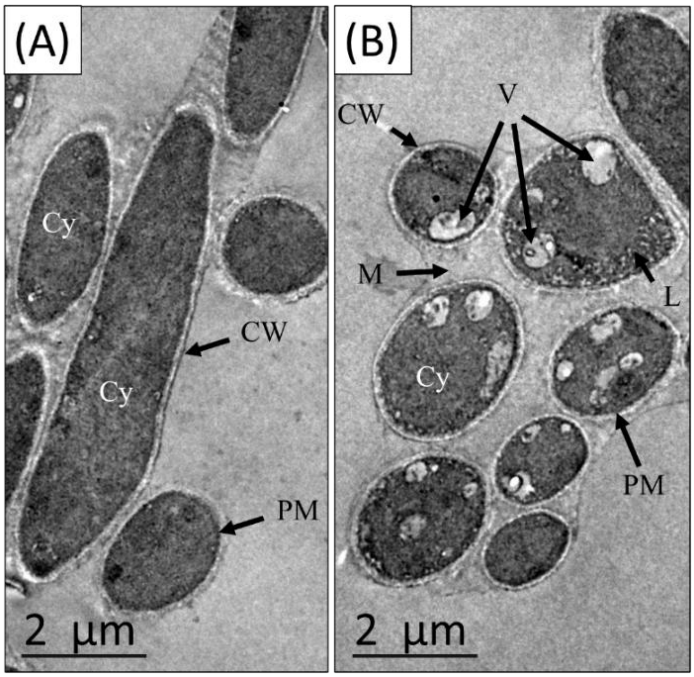

Figure 10 TEM illustrating the impact of the rGO/SiO_2/ZnO nanocomposite on the cellular ultrastructure of *F. oxysporum*. (A) Untreated control hyphae exhibited a healthy, organized architecture with a distinct cell wall (W), intact plasma membrane (PM), small, well-distributed vacuoles (V), and dense, compact cytoplasm (Cy). (B) Treated hyphae demonstrating significant cellular degradation. Notable alterations include the accumulation of dense lipid droplets (L), significant vacuolar expansion (V), and the formation of a prominent extracellular mucilage substance (M), causing hyphal aggregation.

The experimental data reveal a significant dose-dependent response in soybean seedlings, where the 500 mg/L concentration yielded the maximal enhancement in biomass and root system architecture. While this represents the peak performance in the current study, it must be weighed against potential long-term accumulation risks in agricultural soils, as the transition from biostimulation to phytotoxicity often occurs across a narrow threshold in nano-agriculture. Although no immediate phenotypic toxicity—such as leaf chlorosis or root stunting—was observed at 500 mg/L within the controlled setting, this dosage warrants a cautious interpretation regarding sustained field application **(Sagardoy Calderón *et al.*, 2009)**. High dosages of ZnO-based nanocomposites may lead to intracellular stress at which potential over-accumulation of Zn^{2+} ions in plant tissues, which can interfere with essential micronutrient uptake (e.g., Fe and Mg), soil persistence at which cumulative application could lead to the unintended immobilization of NPs in the soil matrix, affecting the rhizospheric microbiome and beneficial soil fungi, or the peripheral edge interaction paradox. While the sharp edges of rGO are effective against *F. oxysporum*, at higher concentrations, they could theoretically impose mechanical stress on the delicate root hair cells of the host plant. Consequently, while 500 mg/L represents the maximal efficacy dose for fungal suppression in this study, we propose that the 150–250 mg/L range may offer a more sustainable equilibrium between growth promotion and environmental safety for field-scale applications.

The observed enhancement in plant vigor likely correlates with the potent antimicrobial action of the nanocomposite. For instance, the rGO/SiO_2/ZnO nanocomposite exhibited a 57% increase in the inhibition zone against *F. oxysporum* compared to monometallic ZnO NPs. This antifungal capacity may allow seedlings to reallocate metabolic resources from defense mechanisms toward developmental processes. Furthermore, the SiO_2 component is suggested to form physical barriers within plant tissues, while zinc acts as a vital cofactor for antioxidant enzymes **(Abdelrhim *et al.*, 2021; Sathiyabama and Indhumathi, 2022)**. These concurrent protective mechanisms may contribute to the statistically significant increases in biomass and node count recorded for the treated seedlings.

Limitations and future outlook

While the rGO/SiO_2/ZnO nanocomposite demonstrated measurable inhibitory efficacy and improved seedling morphometric parameters under controlled conditions, several limitations remain. This study focused on early-stage growth in a greenhouse environment; consequently, field-scale trials are essential to evaluate performance under fluctuating environmental variables. Furthermore, while short-term biostimulatory effects are evident, long-term environmental impact assessments regarding NPs leaching and soil microbial diversity are required. Future research should prioritize the tracking of Zn^{2+} translocation within plant tissues to ensure food safety. To validate the proposed antimicrobial pathways, future studies should focus on direct ROS quantification and advanced microscopy to visualize real-time morphological damage. Additionally, biocompatibility assessments and cytotoxicity assays are recommended to establish safe dosage limits for broader agricultural applications.

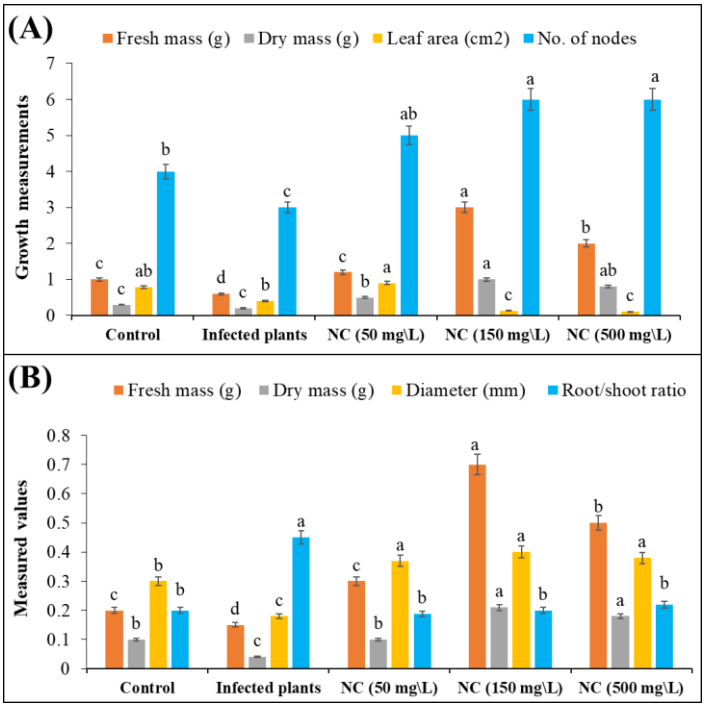

Figure 11 Impact of rGO/SiO_2/ZnO nanocomposite (NC) priming on the growth architecture of soybean (*Glycine max*) seedlings under *F. oxysporum* stress. (A) Shoot growth vigor and phenotypic development; (B) Root system architecture and biomass allocation. Data represent the mean ± SD (n=3 biological replicates). Error bars labeled with different lowercase letters indicate significant differences at $p < 0.05$ according to Tukey's HSD test.

CONCLUSIONS

The global challenge of antimicrobial resistance necessitates the development of effective, non-conventional antimicrobial strategies. This study demonstrated the successful and scalable green synthesis of a novel ternary reduced graphene oxide/silicon dioxide/zinc oxide (rGO/SiO_2/ZnO) nanocomposite mediated by *Glycine max* extract. The synthesized material exhibited significant broad-spectrum antimicrobial activity, notably surpassing the efficacy of ampicillin against the Gram-positive *Bacillus paramycosides*. The observed 3.5-fold increase in inhibitory activity against *Escherichia coli* compared to pristine ZnO NPs suggests a synergistic interaction between the rGO matrix and the anchored metal-oxide nanoparticles. Critically, the integration of time-kill kinetic analysis displayed a rapid, dose-dependent microbicidal effect, with total eradication of *E. coli* observed within 4 hours at 2 × MIC. Furthermore, transmission electron microscopy of treated *Fusarium oxysporum* provided direct ultrastructural evidence of cellular degradation, characterized by expanded vacuolation and lipid droplet accumulation. These findings transition the mechanistic understanding of the rGO/SiO_2/ZnO framework from literature-based hypotheses toward data-driven observations of membrane disruption and internal metabolic stress. In addition to its antimicrobial performance, the material demonstrated potential as a nanobiostimulant. Seed nano-priming significantly enhanced germination rates and early growth vigor in *G. max* under biotic stress from *F. oxysporum*. These multifunctional properties—encompassing both antimicrobial protection and growth enhancement—suggest the potential utility of the rGO/SiO_2/ZnO nanocomposite within the context of sustainable agriculture. Future investigations should prioritize the precise quantification of reactive oxygen species and comprehensive environmental biocompatibility assessments to facilitate the transition of this proof-of-concept into practical field-scale applications.

Ethical approval: The soybean (*Glycine max* L.) seeds (cultivar Giza 21) were obtained from the Agricultural Research Institute (ARI) in Kafr El-Sheikh, Egypt. This cultivated material represents certified agricultural stock and was used in accordance with institutional guidelines and Egyptian national regulations. No

specific permits were required as the material was not wild-harvested or collected from protected areas.

Acknowledgements: The authors thank the staff and administration of the Botany and Microbiology Department at Damietta University for providing the laboratory facilities and general resources necessary to complete this research. This work did not receive any specific grant from funding agencies in the public, commercial, or not-for-profit sectors.

CRediT authorship contribution statement:
Methodology: Mohamed El-Zahed, Manal A. Abdelhamid, and Enas G. Badran; Data Curation and Formal Analysis: Mohamed El-Zahed, Manal A. Abdelhamid, Mamdouh M. Nemat Alla, and Enas G. Badran; Investigation and Resources: Mohamed M. El-Zahed, Manal A. Abdelhamid, Mamdouh M. Nemat Alla, Enas G. Badran; Original draft preparation: Mohamed M. El-Zahed, Manal A. Abdelhamid, Mamdouh M. Nemat Alla, Enas G. Badran; Writing, Reviewing and Editing: Mohamed M. El-Zahed, Manal A. Abdelhamid, Mamdouh M. Nemat Alla, Enas G. Badran; Supervision: Mohamed M. El-Zahed, Mamdouh M. Nemat Alla, Enas G. Badran. All authors read and approved the final manuscript.

Consent for publication
All authors give consent for the publication of the manuscript in the journal "*Journal of Microbiology, Biotechnology and Food Sciences*."

REFERENCES

Abd El-Nour, A. T., Abou-Dobara, M. I., El-Sayed, A. K. A., & El-Zahed, M. M. (2023). Antibacterial activity of optimized extracellular biosynthesized zinc oxide nanoparticles using *Corynebacterium* sp. ATCC 6931. *Scientific Journal of Damietta Faculty of Science*, *13*(1), 63–70. https://doi.org/10.21608/sjdfs.2023.231788.1129

Abdelrhim, A. S., Mazrou, Y. S. A., Nehela, Y., Atallah, O. O., El-Ashmony, R. M., & Dawood, M. F. A. (2021). Silicon dioxide nanoparticles induce innate immune responses and activate antioxidant machinery in wheat against *Rhizoctonia solani*. *Plants*, *10*(12), 2758. https://doi.org/10.3390/plants10122758

Abebe, B., Zereffa, E. A., Tadesse, A., & Murthy, H. C. A. (2020). A review on enhancing the antibacterial activity of ZnO: Mechanisms and microscopic investigation. *Nanoscale Research Letters*, *15*, 190. https://doi.org/10.1186/s11671-020-03418-6

Ahmed, G., Hanif, M., Mahmood, K., Yao, R., Ning, H., Jiao, D., Wu, M., Khan, J., & Liu, Z. (2018). Lattice defects of ZnO and hybrids with GO: Characterization, EPR, and optoelectronic properties. *AIP Advances*, *8*(2), 025218. https://doi.org/10.1063/1.5011356

Ain, Q. T., Al-Modlej, A., Alshammari, A., & Anjum, M. N. (2018). Effect of solvents on the optical band gap of silicon-doped graphene oxide. *Materials Research Express*, *5*(3), 035017. https://doi.org/10.1088/2053-1591/aab239

AL-Azawi, M. T., Hadi, S. M., & Mohammed, C. H. (2019). Synthesis of silica nanoparticles via a green approach by using hot aqueous extract of *Thuja orientalis* leaf and their effect on biofilm formation. *Iraqi Journal of Agricultural Sciences*, *50*(1), 245–255.

Al-Rawashdeh, N. A. F., Allabadi, O., & Aljarrah, M. T. (2020). Photocatalytic activity of graphene oxide/zinc oxide nanocomposites with embedded metal nanoparticles for the degradation of organic dyes. *ACS Omega*, *5*(43), 28046–28055. https://doi.org/10.1021/acsomega.0c03608

Amama, P. B., & Adeoye, S. A. (2026). Catalytic applications of carbon nanotubes in energy and environmental remediation: Multifunctional roles and design strategies. *Nanoscale* (*online accepted manuscript*). https://doi.org/10.1039/D5NR05306D

Atanda, S. A., Shaibu, R. O., & Agunbiade, F. O. (2025). Nanoparticles in agriculture: Balancing food security and environmental sustainability. *Discovery Agriculture*, *3*, 26. https://doi.org/10.1007/s44279-025-00159-x

Baka, Z. A. M., & El-Zahed, M. M. (2023). Biocontrol of chocolate spot disease of broad bean (*Vicia faba* L.) caused by *Botrytis fabae* using biosynthesized reduced graphene oxide/silver nanocomposite. *Physiological and Molecular Plant Pathology*, *127*, 102116. https://doi.org/10.1016/j.pmpp.2023.102116

Baka, Z. A. M., & El-Zahed, M. M. (2022). Antifungal activity of silver/silicon dioxide nanocomposite on the response of faba bean plants (*Vicia faba* L.) infected by *Botrytis cinerea*. *Bioresources and Bioprocessing*, *9*, 102. https://doi.org/10.1186/s40643-022-00591-7

Baka, Z. A. M., El-Sharkawy, A. M., & El-Zahed, M. M. (2024). Anti-*Aspergillus niger* action of biosynthesized silicon dioxide nanoparticles alone or combined with *Matricaria chamomilla* L. extract. *Journal of Microbiology, Biotechnology and Food Sciences*, *13*(5), e10816. https://doi.org/10.55251/jmbfs.10816

Banerjee, S., Roy, P., Nandi, S., & Roy, S. (2023). Advanced biotechnological strategies towards the development of crops with enhanced micronutrient content. *Plant Growth Regulation*, *100*, 355–371. https://doi.org/10.1007/s10725-023-00968-4

Bouhadi, M., Javed, Q., Jakubus, M., Elkouali, M., Fougrach, H., Ansar, A., Ban, S. G., Ban, D., Heath, D., & Černe, M. (2025). Nanoparticles for sustainable agriculture: Assessment of benefits and risks. *Agronomy*, *15*(5), 1131. https://doi.org/10.3390/agronomy15051131

Budran, E. G., Abdelhamid, M. A., Hassan, N. M., & Nemat Alla, M. M. (2023). Improving fatty acid composition of soybean yield under NaCl stress by soaking seeds in ascorbate. *Acta Physiologiae Plantarum*, *45*, 75. https://doi.org/10.1007/s11738-023-03555-2

Chowdhuri, A. R., Tripathy, S., Chandra, S., Roy, S., & Kumar Sahu, S. (2015). A ZnO decorated chitosan–graphene oxide nanocomposite shows significantly enhanced antimicrobial activity with ROS generation. *RSC Advances*, *5*(61), 49420–49428. https://doi.org/10.1039/C5RA05393E

CLSI (Clinical and Laboratory Standards Institute). (1999). *Methods for Determining Bactericidal Activity of Antimicrobial Agents; Approved Guideline*. CLSI document M26-A. Clinical and Laboratory Standards Institute, Wayne, PA, USA.

CLSI (2017). *Performance Standards for Antimicrobial Susceptibility Testing: Approved Standard-Twenty-Seven Edition (M100-S26)*. Clinical and Laboratory Standards Institute, Wayne, PA, USA.

Sani, G. D., Yakubu, A., Saidu, A., Aati, R., Sahabi, S., & Sirajo, A. (2023). A review on industrial applications of zinc oxide nanoparticles. *International Journal of Advanced Rheumatology*, *5*(1), 2395–5252. https://doi.org/10.35629/5252-050110311041

de Medeiros, A. M. Z., Khan, L. U., da Silva, G. H., Ospina, C. A., Alves, O. L., de Castro, V. L., & Martinez, D. S. T. (2021). Graphene oxide-silver nanoparticle hybrid material: An integrated nanosafety study in zebrafish embryos. *Ecotoxicology and Environmental Safety*, *209*, 111776. https://doi.org/10.1016/j.ecoenv.2020.111776

Naghani, E. M., Neghabi, M., Zadsar, M., & Abbastabar Ahangar, H. (2023). Synthesis and characterization of linear/nonlinear optical properties of graphene oxide and reduced graphene oxide-based zinc oxide nanocomposite. *Scientific Reports*, *13*, 1496. https://doi.org/10.1038/s41598-023-28307-7

Elbasuney, S., El-Sayyad, G. S., Tantawy, H., & Hashem, A. H. (2021). Promising antimicrobial and antibiofilm activities of reduced graphene oxide-metal oxide (RGO-NiO, RGO-AgO, and RGO-ZnO) nanocomposites. *RSC Advances*, *11*(41), 25961–25975. https://doi.org/10.1039/D1RA04542C

Elemike, E. E., & Ivwurie, W. (2020). Current green nanotechnology: The case of noble metal nanocomposites and applications. In: Saquib, Q., Faisal, M., Al-Khedhairy, A.A., Alatar, A.A. (Eds.), Green Synthesis of Nanoparticles: Applications and Prospects (pp. 23-51). Singapore: Springer Singapore. https://doi.org/10.1007/978-981-15-5179-6_2

El-Fallal, A. A., Elfayoumy, R. A., & El-Zahed, M. M. (2023). Antibacterial activity of biosynthesized zinc oxide nanoparticles using Kombucha extract. *SN Applied Sciences*, *5*, 332. https://doi.org/10.1007/s42452-023-05546-x

Elumalai, K., & Velmurugan, S. (2015). Green synthesis, characterization and antimicrobial activities of zinc oxide nanoparticles from the leaf extract of *Azadirachta indica* (L.). *Applied Surface Science*, *345*, 329–336. https://doi.org/10.1016/j.apsusc.2015.03.176

El-Zahed, M. M., Baka, Z. A. M., El-Sayed, A. K., & Abou-Dobara, M. I. (2022). The anti-*Aspergillus* potential of optimized biosynthesized reduced graphene oxide/silver nanocomposite using *Escherichia coli* D8 (MF062579). *Journal of Microbiology, Biotechnology and Food Sciences*, 12(2), e5864. https://doi.org/10.55251/jmbfs.5864

El-Zahed, A. A. Z., Khalifa, M. E., El-Zahed, M. M., & Baka, Z. A. (2023). Biological synthesis and characterization of antibacterial manganese oxide nanoparticles using *Bacillus subtilis* ATCC 6633. *Scientific Journal of Damietta Faculty of Science*. https://doi.org/10.21608/sjdfs.2023.242279.1136

El-Zahed, M. M., Abou-Dobara, M. I., El-Khodary, M. M., & Mousa, M. M. A. (2024). Antimicrobial activity and nanoremediation of heavy metals using biosynthesized CS/GO/ZnO nanocomposite by *Bacillus subtilis* ATCC 6633 alone or immobilized in a macroporous cryogel. *Microbial Cell Factories*, *23*, 278. https://doi.org/10.1186/s12934-024-02535-6

Esmailzadeh, H., Sangpour, P., Shahraz, F., Hejazi, J., & Khaksar, R. (2016). Effect of nanocomposite packaging containing ZnO on growth of *Bacillus subtilis* and *Enterobacter aerogenes*. *Materials Science and Engineering: C*, *58*, 1058–1063. https://doi.org/10.1016/j.msec.2015.09.078

Faizan, M., Bhat, J. A., Chen, C., Alyemeni, M. N., Wijaya, L., Ahmad, P., & Yu, F. (2021). Zinc oxide nanoparticles (ZnO-NPs) induce salt tolerance by improving the antioxidant system and photosynthetic machinery in tomato. *Plant Physiology and Biochemistry*, *161*, 122–130. https://doi.org/10.1016/j.plaphy.2021.02.002

Farhana, Munis, M. F. H., Alamer, K. H., Althobaiti, A. T., Kamal, A., Liaquat, F., Haroon, U., Ahmed, J., Chaudhary, H. J., & Attia, H. (2022). ZnO nanoparticle-mediated seed priming induces biochemical and antioxidant changes in chickpea to alleviate Fusarium wilt. *Journal of Fungi*, *8*(7), 753. https://doi.org/10.3390/jof8070753

Fayed, R. M., Baka, Z. A. M., Farouk, B. H., & El-Zahed, M. M. (2025). Antibacterial and cytotoxic activities of a newly green synthesized ZnO/Se nanocomposite combined with *Washingtonia robusta* H. Wendl fruit extract. *Biocatalysis and Agricultural Biotechnology*, *64*, 103500. https://doi.org/10.1016/j.bcab.2025.103500

Gautam, A., Dabral, H., Singh, A., Tyagi, S., Tyagi, N., Srivastava, D., Kushwaha, H. R., & Singh, A. (2024). Graphene-based metal/metal oxide nanocomposites as

potential antibacterial agents: A mini-review. *Biomaterials Science*, 12(18), 4630-4649. https://doi.org/10.1039/D4BM00796D
Gijare, M., Chaudhari, S., Ekar, S., Shaikh, S. F., Mane, R. S., Pandit, B., Siddiqui, M. U. H., & Garje, A. (2023). Facile green preparation of reduced graphene oxide using *Citrus limetta*-decorated rGO/TiO2 nanostructures for glucose sensing. *Electronics*, *12*(2), 294. https://doi.org/10.3390/electronics12020294
Goswami, P., & Mathur, J. (2022). Application of agro-waste-mediated silica nanoparticles to sustainable agriculture. *Bioresources and Bioprocessing.*, *9*, 9. https://doi.org/10.1186/s40643-022-00496-5
Guo, X., Zhang, Q., Ding, X., Shen, Q., Wu, C., Zhang, L., & Yang, H. (2016). Synthesis and application of several sol–gel-derived materials via sol–gel process combining with other technologies: A review. *Journal of Sol-Gel Science and Technology*, *79*, 328–358. https://doi.org/10.1007/s10971-015-3935-6
Hayat, M. A. (Ed.) (1981). 7 - Methods of Fixation. In: *Fixation for electron microscopy* (pp. 200-208). Academic Press Inc., Elsevier. https://doi.org/10.1016/B978-0-12-333920-1.50011-2
Hindersah, R., Setiawati, M. R., Fitriatin, B. N., Suryatama, P., Asmiran, P., Panatarani, C., & Joni, I. M. (2018). Graphite tail powder and liquid biofertilizer as a source of trace elements for ground nut. *AIP Conference Proceedings*, *1927*(1), 030004. https://doi.org/10.1063/1.5021197
Hudson, J. P. (1967). Sand and water culture methods used in the study of plant nutrition. *Experimental Agriculture*, *3*(2), 104. https://doi.org/10.1017/S0014479700021852
Jafari, A. J., Kalantary, R. R., Esrafili, A., & Arfaeinia, H. (2018). Synthesis of silica-functionalized graphene oxide/ZnO coated on fiberglass and its application in photocatalytic removal of gaseous benzene. *Process Safety and Environmental Protection*, *116*, 377–387. https://doi.org/10.1016/j.psep.2018.03.015
Kamal, A., Yang, J., Batool, M., Ara, U., Khattak, W. A., Touhami, D., Aljowaie, R. M., & Elshikh, M. S. (2024). Green synthesis of zinc oxide nanoparticles, characterization and its applications in inducing disease resistance against spot blot disease in wheat by enhancing its physiological and biochemical parameters. *Journal of Crop Health*, *77*, 5. https://doi.org/10.1007/s10343-024-01088-3
Karthiga, P., Chitra, K., Wadaan, M. A., Mythili, R., Lee, J., & Bharathi, D. (2025). Green synthesis of ZnO nanoparticles using *Ficus benghalensis* for visible light–driven photocatalytic degradation of crystal violet and antibacterial and antibiofilm activities. *Luminescence*, *40*(1), e70088. https://doi.org/10.1002/bio.70088
Kim, Y. H., Khan, A. L., & Lee, I. J. (2016). Silicon: A duo synergy for regulating crop growth and hormonal signaling under abiotic stress conditions. *Critical Reviews in Biotechnology*, *36*(6), 1099–1109. https://doi.org/10.3109/07388551.2015.1084265
Kumar, P., Huo, P., Zhang, R., & Liu, B. (2019). Antibacterial properties of graphene-based nanomaterials. *Nanomaterials*, *9*(5), 737. https://doi.org/10.3390/nano9050737
Lavkush Bhaisare, M., Wu, B. S., Wu, M. C., Shahnawaz Khan, M., Tseng, M. H., & Wu, H. F. (2016). MALDI MS analysis, disk diffusion and optical density measurements for the antimicrobial effect of zinc oxide nanorods integrated in graphene oxide nanostructures. *Biomaterials Science*, *4*(1), 183–194. https://doi.org/10.1039/C5BM00342C
Li, M., Zou, L., Zhang, L., Ren, G., Liu, Y., Zhao, X., & Qin, P. (2025). Plant-based proteins: Advances in their sources, digestive profiles in vitro and potential health benefits. *Critical Reviews in Food Science and Nutrition*, *65*(10), 1929–1949. https://doi.org/10.1080/10408398.2024.2315448
Lindsay, W. L. (1972). Zinc in soils and plant nutrition. In: Brady, N. C. (Ed.), *Advances in Agronomy* (pp. 147–186). Academic Press INC. Elsevier. https://doi.org/10.1016/S0065-2113(08)60635-5
Liu, R., & Lal, R. (2015). Potentials of engineered nanoparticles as fertilizers for increasing agronomic productions. *Science of The Total Environment*, *514*, 131–139. https://doi.org/10.1016/j.scitotenv.2015.01.104
Liu, S., Zeng, T. H., Hofmann, M., Burcombe, E., Wei, J., Jiang, R., Kong, J., & Chen, Y. (2011). Antibacterial activity of graphite, graphite oxide, graphene oxide, and reduced graphene oxide: Membrane and oxidative stress. *ACS Nano*, *5*(9), 6971–6980. https://doi.org/10.1021/nn202451x
Madan, H. R., Sharma, S. C., Udayabhanu, Suresh, D., Vidya, Y. S., Nagabhushana, H., Rajanaik, H., Anantharaju, K. S., Prashantha, S. C., & Sadananda Maiya, P. (2016). Facile green fabrication of nanostructure ZnO plates, bullets, flower, prismatic tip, closed pine cone: Their antibacterial, antioxidant, photoluminescent and photocatalytic properties. *Spectrochimica Acta Part A: Molecular and Biomolecular Spectroscopy*, *152*, 404–416. https://doi.org/10.1016/j.saa.2015.07.067
Mahdavi, H., Kerachian, M. A., & Abazari, M. (2022). Synergistic effect of GO@SiO2 and GO@ZnO nano-hybrid particles with PVDF-g-PMMA copolymer in high-flux ultrafiltration membrane for oily wastewater treatment and antifouling properties. *Journal of Industrial and Engineering Chemistry*, *108*, 374–388. https://doi.org/10.1016/j.jiec.2022.01.016
Majumder, D. D., Banerjee, R., Ulrichs, C. H., Mewis, I., & Goswami, A. (2007). Nano-materials: Science of bottom-up and top-down. *IETE Technical Review*, *24*(1), 9–25. https://doi.org/10.4103/02564602.10876577
Maroni, F., Raccichini, R., Birrozzi, A., Carbonari, G., Tossici, R., Croce, F., Marassi, R., & Nobili, F. (2014). Graphene/silicon nanocomposite anode with enhanced electrochemical stability for lithium-ion battery applications. *Journal of Power Sources*, *269*, 873–882. https://doi.org/10.1016/j.jpowsour.2014.07.064
Mohd Yusof, H., Abdul Rahman, N., Mohamad, R., Zaidan, U. H., & Samsudin, A. A. (2020). Biosynthesis of zinc oxide nanoparticles by cell-biomass and supernatant of *Lactobacillus plantarum* TA4 and its antibacterial and biocompatibility properties. *Scientific Reports*, *10*, 19996. https://doi.org/10.1038/s41598-020-76402-w
Musa, I., & Qamhieh, N. (2019). Study of optical energy gap and quantum confinement effects in zinc oxide nanoparticles and nanorods. *Digest Journal of Nanomaterials and Biostructures. 14*, 119-125.
Naser, M., Abdelghany, A. M., Wu, T., Sun, S., & Tianfu, H. (2024). Soybean in Egypt: Current situation, challenges, and future perspectives. *Discovery Sustainability*, *5*, 425. https://doi.org/10.1007/s43621-024-00656-x
Nour El-Dein, M. M., Baka, Z. A. M., Abou-Dobara, M. I., El-Sayed, A. K., & El-Zahed, M. M. (2021). Extracellular biosynthesis, optimization, characterization and antimicrobial potential of *Escherichia coli* D8 silver nanoparticles. *Journal of Microbiology, Biotechnology and Food Sciences*, *10*(4), 648–656. https://doi.org/10.15414/jmbfs.2021.10.4.648-656
O'connor, B. P. (2000). SPSS and SAS programs for determining the number of components using parallel analysis and Velicer's MAP test. *Behavior Research Methods, Instruments, & Computers*, *32*(3), 396–402. https://doi.org/10.3758/BF03200807
Pandorf, M., Pourzahedi, L., Gilbertson, L., Lowry, V. G., Herckes, P., & Westerhoff, P. (2020). Graphite nanoparticle addition to fertilizers reduces nitrate leaching in growth of lettuce (*Lactuca sativa*). *Environmental Science: Nano*, *7*(1), 127–138. https://doi.org/10.1039/C9EN00890J
Patel, J. B., Tenover, F. C., Turnidge, J. D., & Jorgensen, J. H. (2011). Susceptibility test methods: Dilution and disk diffusion methods. In: *Manual of Clinical Microbiology*. John Wiley & Sons, Ltd, pp. 1122–1143. https://doi.org/10.1128/9781555816728.ch68
Pedruzzi, D. P., Araujo, L. O., Falco, W. F., Machado, G., Casagrande, G. A., Colbeck, I., Lawson, T., Oliveira, S. L., & Caires, A. R. L. (2020). ZnO nanoparticles impact on the photosynthetic activity of *Vicia faba*: Effect of particle size and concentration. *NanoImpact*, *19*, 100246. https://doi.org/10.1016/j.impact.2020.100246
Qian, K., Kumar, A., Zhang, H., Bellmer, D., & Huhnke, R. (2015). Recent advances in utilization of biochar. *Renewable and Sustainable Energy Reviews*, *42*, 1055–1064. https://doi.org/10.1016/j.rser.2014.10.074
Qin, P., Wang, T., & Luo, Y. (2022). A review on plant-based proteins from soybean: Health benefits and soy product development. *Journal of Agriculture and Food Research*, *7*, 100265. https://doi.org/10.1016/j.jafr.2021.100265
Rafique, S., Bashir, S., Akram, R., Jawaid, S., Bashir, M., Aftab, A., Attique, A., & Awan, S. U. (2023). In vitro anticancer activity and comparative green synthesis of ZnO/Ag nanoparticles by *Moringa oleifera*, *Mentha piperita*, and *Citrus lemon*. *Ceramics International*, *49*(4), 5613–5620. https://doi.org/10.1016/j.ceramint.2022.10.163
Rosnan, N. A., Haan, T. Y., & Mohammad, A. W. (2018). Synthesis and characterization of ZnO-decorated GO nanocomposite material with different ZnO loading through sol-gel method. *Jurnal Kejuruteraan*, *30*(2), 249–255. https://doi.org/10.17576/jkukm-2018-30(2)-15
Safajou, H., Mizwari, Z. M., Rostaminia, A., Khojasteh, H., Aspoukeh, P., & Mazhari, M. P. (2025). Green synthesis and enhanced photocatalytic performance of rGO/ZnO/Fe3O4 nanocomposites: A sustainable approach to environmental remediation. *Journal of Fluorescence*, *35*, 6409–6428. https://doi.org/10.1007/s10895-024-04014-y
Sagardoy Calderón, R., Morales, F., López-Millán, A. F., Abadía Bayona, A., & Abadía Bayona, J. (2009). Effects of zinc toxicity on sugar beet (*Beta vulgaris* L.) plants grown in hydroponics. *Plant Biology*, *11*(3), 339-350.
Salem, S. S., & Fouda, A. (2021). Green synthesis of metallic nanoparticles and their prospective biotechnological applications: An overview. *Biological Trace Element Research*, *199*, 344–370. https://doi.org/10.1007/s12011-020-02138-3
Sathiyabama, M., & Indhumathi, M. (2022). Chitosan thiamine nanoparticles intervene innate immunomodulation during chickpea-*Fusarium* interaction. *International Journal of Biological Macromolecules*, *198*, 11–17. https://doi.org/10.1016/j.ijbiomac.2021.12.105
Seleiman, M. F., Refay, Y., Al-Suhaibani, N., Al-Ashkar, I., El-Hendawy, S., & Hafez, E. M. (2019). Integrative effects of rice-straw biochar and silicon on oil and seed quality, yield and physiological traits of *Helianthus annuus* L. grown under water deficit stress. *Agronomy*, *9*(10), 637. https://doi.org/10.3390/agronomy9100637
Shabiya, A., Bhat, M. A., Singh, P., Hassan, S., & Hussain, N. (2025). Nanofertilizers: Mechanisms, efficacy, and implications for sustainable agriculture. In: Hussain, N., Hung, C. Y., & Wang, L. (Eds.), *Agricultural Nutrient Pollution and Climate Change: Challenges and Opportunities* (pp. 311–353). Springer Nature, Cham, . https://doi.org/10.1007/978-3-031-80912-5_11
Shafey, A. M. E. (2020). Green synthesis of metal and metal oxide nanoparticles from plant leaf extracts and their applications: A review. *Green Processing and Synthesis*, *9*(1), 304–339. https://doi.org/10.1515/gps-2020-0031

Sharma, A., Patni, B., Shankhdhar, D., & Shankhdhar, S. C. (2013). Zinc – An indispensable micronutrient. *Physiology and Molecular Biology of Plants*, *19*(1), 11–20. https://doi.org/10.1007/s12298-012-0139-1

Simões, M., Simões, L. C., & Vieira, M. J. (2010). A review of current and emergent biofilm control strategies. *LWT - Food Science and Technology*, *43*(4), 573–583. https://doi.org/10.1016/j.lwt.2009.12.008

Singh, N., & Das, P. P. (2024). Role and application of graphene nanomaterial in crop improvement and the enhancement of productivity of crops. In: *Graphene-Based Nanomaterials*. CRC Press.

Singh, P., Singh, A. K., Singh, V. K., & Kumar, V. (2025). *Nanotechnology-based Sustainable Agriculture*. Wiley Online Books, Wiley.

Sri Sindhura, K., Prasad, T. N. V. K. V., Panner Selvam, P., & Hussain, O. M. (2014). Synthesis, characterization and evaluation of effect of phytogenic zinc nanoparticles on soil exo-enzymes. *Applied Nanoscience*, *4*(7), 819–827. https://doi.org/10.1007/s13204-013-0263-4

Stanković, A., Dimitrijević, S., & Uskoković, D. (2013). Influence of size scale and morphology on antibacterial properties of ZnO powders hydrothermally synthesized using different surface stabilizing agents. *Colloids and Surfaces B: Biointerfaces*, *102*, 21–28. https://doi.org/10.1016/j.colsurfb.2012.07.033

Toselli, M., Fabiani, D., Mancinelli, P., Fréchette, M., Heid, T., David, E., & Saccani, A. (2015). In situ thermal reduction of graphene oxide forming epoxy nanocomposites and their dielectric properties. *Polymer Composites*, *36*(2), 294–301. https://doi.org/10.1002/pc.22943

Ullah, A., & Lim, S. I. (2022). Plant extract-based synthesis of metallic nanomaterials, their applications, and safety concerns. *Biotechnology and Bioengineering*, *119*(9), 2273–2304. https://doi.org/10.1002/bit.28148

Umar, H., Kavaz, D., & Rizaner, N. (2019). Biosynthesis of zinc oxide nanoparticles using *Albizia lebbeck* stem bark, and evaluation of its antimicrobial, antioxidant, and cytotoxic activities on human breast cancer cell lines. *International Journal of Nanomedicine*, *14*, 87–100. https://doi.org/10.2147/IJN.S186888

Wang, X., Yang, X., Chen, S., Li, Q., Wang, W., Hou, C., Gao, X., Wang, L., & Wang, S. (2016). Zinc oxide nanoparticles affect biomass accumulation and photosynthesis in *Arabidopsis*. *Frontiers in Plant Science*, *6*, 1243. https://doi.org/10.3389/fpls.2015.01243

Wang, Y. W., Cao, A., Jiang, Y., Zhang, X., Liu, J. H., Liu, Y., & Wang, H. (2014). Superior antibacterial activity of zinc oxide/graphene oxide composites originating from high zinc concentration localized around bacteria. *ACS Applied Materials & Interfaces*, *6*(4), 2791–2798. https://doi.org/10.1021/am4053317

Youssif, N. E. E., Osman, H. S. M., Salama, Y. A. M., & Zaghlool, S. A. M. (2018). Effect of rice straw and applications of potassium silicate, potassium humate and seaweed extract on growth and some macronutrients of sweet pepper plants under irrigation deficit. *Arab Universities Journal of Agricultural Sciences*, *26*(1), 1-15. https://doi.org/10.21608/ajs.2018.16008